POLITECNICO DI TORINO
Repository ISTITUZIONALE

Beam Scheduling for Multi-Connectivity NTN LEO D2C Satellite Networks

Original
Beam Scheduling for Multi-Connectivity NTN LEO D2C Satellite Networks / Wang, J., Kong, D., Guo, Q., Taricco, G.. - (2026), pp. 1-6. (2026 IEEE 103rd Vehicular Technology Conference (VTC2026-Spring) Nice (Fra) 09-12 June 2026) [10.1109/vtc2026-spring68026.2026.11757707].

Availability:
This version is available at: 11583/3018033 since: 2026-11-18T13:13:14Z

Publisher:
IEEE

Published
DOI:10.1109/vtc2026-spring68026.2026.11757707

Terms of use:

This article is made available under terms and conditions as specified in the corresponding bibliographic description in the repository

Publisher copyright
IEEE postprint/Author's Accepted Manuscript

©2026 IEEE. Personal use of this material is permitted. Permission from IEEE must be obtained for all other uses, in any current or future media, including reprinting/republishing this material for advertising or promotional purposes, creating new collecting works, for resale or lists, or reuse of any copyrighted component of this work in other works.

(Article begins on next page)

29 November 2026

Beam Scheduling for Multi-Connectivity NTN LEO D2C Satellite Networks

Junru Wang*, Deyu Kong*, Qing Guo*, Giorgio Taricco†
*School of Electronic and Information Engineering, Harbin Institute of Technology, Harbin 150001, China
Email: jr.wang@stu.hit.edu.cn, hunterkong1997@gmail.com, qguo@hit.edu.cn
†Dipartimento di Elettronica e Telecomunicazioni, Politecnico di Torino, 10129 Turin, Italy
Email: giorgio.taricco@polito.it

***Abstract*—Low Earth Orbit (LEO) satellite constellations are increasingly deployed to bridge connectivity gaps in remote and underserved areas, with Direct-to-Cell (D2C) services enabling smartphones to directly connect to satellites. However, the non-uniform user distributions lead to substantial mismatches between traffic demand and available data rate, especially in hotspot regions. Motivated by these challenges, we propose a beam scheduling framework for multi-satellite multi-connectivity in LEO Non-Terrestrial Networks (NTN), leveraging New Radio (NR) features for concentrated multi-beam illumination under the capability assumptions of NR cellphones. We address the multi-connectivity beam schedule problem by proposing a cell-proposed deferred acceptance matching scheme that generates sparse inputs for a mixed-integer programming solver. Numerical results demonstrate that the proposed multi-connectivity framework improves demand matching and fairness compared to conventional single-connectivity beam scheduling. The results indicate that integrating multi-connectivity with NTN features can effectively overcome existing limitations in spectral efficiency and fairness, providing a compelling motivation for satellite operators to transition to NTN for future D2C deployments.**

***Index Terms*—LEO satellite communication, non-terrestrial networks, multi-connectivity, resource management, non-uniform demand**

I. Introduction

Low Earth Orbit (LEO) satellites provide lower propagation delays and reduced signal losses compared to Geostationary Earth Orbit (GEO) satellites, complementing existing terrestrial cellular base stations to achieve 99% global coverage. D2C services started using adapted LTE standards allowing smartphones to directly connect to satellite networks in coverage gaps.

Due to wide-area satellite beam footprints and limited available bandwidth, full frequency reuse (FFR) strategies cannot effectively address traffic imbalances in hotspot regions [1]. Beam scheduling methods (i.e., beam illumination pattern design) based on the beam hopping (BH) technique have been studied [2] for multiplexing beams while avoiding self-interference. However, this technique still struggles to meet traffic demands in hotspot areas.

Multi-connectivity transmission, which means serving each user from multiple cooperating access points, can be applied to LEO constellations to significantly improve peak spectral efficiency [3], [4]. However, existing methods exhibit several limitations. First, D2C-specific scenarios are underexplored. Power gain can only be harvested through signal superposition [5]. More critically, user-centric considerations are lacking. In [4], users are sequentially scheduled over possible links, introducing a first-mover advantage that depletes satellite resources for later users. While [6] utilizes swap-based negotiation [7] for the single-connectivity case to mitigate this, each swap requires the total utility verification, which still results in inefficient exploration of the enormous solution space.

In this paper, we propose a multi-satellite multi-connectivity beam scheduling framework for NTN LEO D2C scenarios. The design leverages existing NR/NTN features to enable concentrated multi-beam illumination through cell-level pre-compensation and non-coherent combining on commercial NR smartphones. A cell-proposed deferred acceptance matching algorithm generates beam pattern candidates, which are further optimized using a mixed-integer programming approach. Simulation results show that introducing multi-connectivity improves the system's ability to match satellite beams with spatially uneven user demands while enhancing fairness.

II. System Model and Problem Formulation

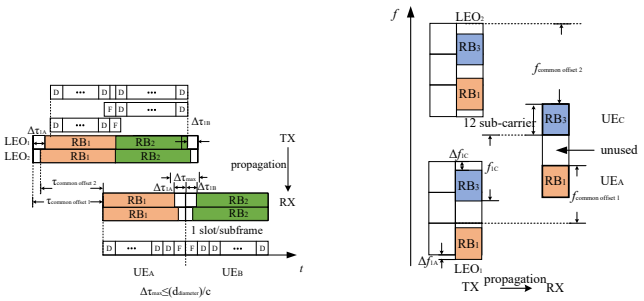
A. NTN LEO D2C architecture

We consider a region consisting of spatially correlated cells $[M] \triangleq \{1, \ldots, M\}$. A satellite beam cell is a hexagon inscribed within the nadir-projected circular boundary of a spot beam footprint. We adopt the earth-fixed cell configuration.

From a cell-centric perspective, let $\mathcal{F}_m$ denote the set of LEO satellites visible to cell m, defined by the field of view (FoV) corresponding to the minimum elevation angle ϵ. We let $\cup_{m=1}^{M} \mathcal{F}_m = [N]$ denote the set of LEO satellites serving the region. Due to visibility reciprocity, each satellite n serves a subset of cells, denoted by $\tilde{\mathcal{F}}_n$. Cells are covered by multiple LEO satellites, implying that $|\mathcal{F}_m| > 1$, thereby enabling multi-connectivity transmission. The number of concurrently multiplexed beams for each satellite $n \in [N]$ is limited by Q_n. FFR is employed to enhance the spectral efficiency. The NTN architecture adopts a centralized unit (CU) and distributed unit (DU) split, where beam scheduling is centrally executed at the CU. Consistent with centralized optimization, reliable cross-cell CSI from all beams is assumed available at the CU.

Multi-satellite D2C transmission requires precise time-frequency synchronization. This ensures that user terminals

Corresponding author: Qing Guo (qguo@hit.edu.cn)



(a) (b)

Fig. 1. Illustration of NTN D2C multi-connectivity transmissions: (a) NR flexible frame and (b) RB fragmentation compatible with existing NR protocols.

within each beam cell can combine signals from multiple satellites. 3GPP NTN systems apply a common onboard pre-compensation aligned with the geographic center of each cell [8]. Inspired by [9], we employ flexible NR slot configurations (Fig. 1a) and RB fragmentation (Fig. 1b), enabling aligned scheduling and non-coherent signal-power superposition at the receiver.

B. Problem Definition

Formally, we discretize the scheduling period into time slots $[T] \triangleq \{1, \ldots, T\}$. Let $x^t_{m,n} \in \{0, 1\}$ denote the connection state between cell m and satellite n in time slot t. The beam scheduling problem is formulated for the downlink transmission scenario. Multi-satellite reception is modeled as non-coherent power accumulation rather than coherent transmission, in contrast to the assumptions of terrestrial studies [10]. Thus, only received powers add across satellites, and the achievable data rate for cell m at time slot t is given by

$$R_m(t) = \omega_m \log\Bigg(1+ \frac{\sum_{n\in[N]} x^t_{m,n}|h_{m,n}|^2 P_{tx}}{\sum_{j\neq m}\sum_{n\in[N]} x^t_{m,n}|h_{m,n}|^2 P_{tx} + \sigma^2_m}\Bigg). \tag{1}$$

Here, P_{tx}, $\sigma^2_m = N_o\omega_m$, and $\omega_m = (N_{RB} - \max\{N^m_{UE} - 1, 0\})B_{RB}$ denote transmit power, noise power, and usable bandwidth after guard RB removal, respectively. N^m_{UE} is the number of active UEs in cell m, N_{RB} is the total number of resource blocks (RBs) within the channel bandwidth, and B_{RB} is the bandwidth of a single RB. The average rate $R_{\text{avg},m}$ for cell m over T time slots is defined as

$$R_{\text{avg},m} = \frac{1}{T}\sum_{t=1}^{T} R_m(t)$$

In the following, we define the Offered Capacity to Traffic Ratio (OCTR) [2], [11] for cell m as $\eta_m = \frac{R_{\text{avg},m}}{D_m}, \forall m \in [M]$, evaluating how the scheduled rate matches the traffic demand over one scheduling period. We further define the minimum OCTR across all cells, expressed as $\eta = \min_{m\in\mathcal{M}} \eta_m$, which is equivalent to the set of linear constraints $\eta_m \geq \eta, \forall m \in [M]$. The demand matching problem can be formulated as an Integer NonLinear Programming (INLP) problem:

Problem 1:

$$\begin{aligned} &\underset{x^t_{m,n}}{\text{maximize}}\ \eta \\ \text{s.t.}\quad &\sum_{m\in\tilde{\mathcal{F}}_n} x^t_{m,n} \leq Q_n,\ \forall n \in [N] && \text{(2a)} \\ &x^t_{m,n} \in \{0, 1\}, \forall n \in [N], \forall m \in [M], \forall t \in [T] && \text{(2b)} \end{aligned}$$

Here, D_m is the data rate demand of cell m.

Define the rate matrix $\mathbf{R} = [\mathbf{r}_1, \ldots, \mathbf{r}_V]$, where each column $\mathbf{r}_v = [\mathcal{R}_1(v), \ldots, \mathcal{R}_M(v)]^{\mathrm{T}}$ represents the rate vector corresponding to beam pattern $v \in [V] \triangleq \{1, \ldots, V\}$. The instantaneous rate of cell m is expressed as $\mathcal{R}_m(v)$ under beam pattern v. Furthermore, let ϕ_v denote the slot-occupancy—that is, the number of slots when the rate pattern v is selected within a complete scheduling period.

Then, the average rate for cell m can also be expressed as

$$R_{\text{avg},m} = \frac{1}{T}\sum_{v=1}^{V} \phi_v\, \mathcal{R}_m(v), \quad \forall m \in [M] \tag{3}$$

This problem can be transformed into a Mixed-Integer Linear Programming (MILP) problem.

Problem 2:

$$\begin{aligned} &\underset{\phi_1,\ldots,\phi_V}{\text{maximize}}\ \eta \quad \text{s.t.} && \sum_{v=1}^{V} \phi_v = T, \phi_v \in \mathbb{N} && \text{(4a)} \\ & && \eta_m \geq \eta, \quad \forall m \in [M] && \text{(4b)} \end{aligned}$$

Next, we determine the demand-matching beam patterns as inputs to the MILP.

III. Algorithm Design

This section illustrates the algorithms proposed in this work, namely, i) the cell-proposed recursive pattern-search algorithm and ii) the deferred acceptance matching algorithm.

A. Cell-proposed algorithm by recursive pattern search

In a multiple LEO satellites scenario, the associations between satellite beams and cells are to be determined. Since demand matching must consider the limitations of satellite capacity (2a), we design a two-stage cell-proposed deferred acceptance matching scheme inspired by [12]. The functions $\psi_m : |\mathcal{F}_m| \mapsto \mathcal{F}_m$ will be used to extract the p-th satellite index in the set $\mathcal{F}_m$. From a cell-centric perspective, we rearrange binary connection state $x^v_{m,p}$ for each cell m. Dropping the pattern index v, we perform a variable substitution by defining $a^2_{m,p} = x^v_{m,p} = x_{m,p}$. Then, define the two vectors $\mathbf{a}_m \triangleq [a_{m,1}, \ldots, a_{m,|\mathcal{F}_m|}]^{\mathrm{T}}$ and $\mathbf{h}_{j,\mathcal{F}_m} \triangleq [h_{j,\psi_m(1)}, \ldots, h_{j,\psi_m(|\mathcal{F}_m|)}]^{\mathrm{T}}$ (channel vector for cell j). The instantaneous rate can be expressed as follow (here, $\odot$ denotes element-wise multiplication):

$$R_m(\mathbf{a}_m) = \omega_m \log\Bigg(1 + \frac{\mathbf{a}^T_m \operatorname{diag}\big(\mathbf{h}^*_{m,\mathcal{F}_m} \odot \mathbf{h}_{m,\mathcal{F}_m}\big)\mathbf{a}_m}{\sum_{j\neq m}\mathbf{a}^T_j \operatorname{diag}\big(\mathbf{h}^*_{m,\mathcal{F}_j} \odot \mathbf{h}_{m,\mathcal{F}_j}\big)\mathbf{a}_j + \sigma^2/P_{tx}}\Bigg). \tag{5}$$

We introduce another metric that quantifies how closely the currently achieved rate matches traffic demand:

$$\eta_m(v) \triangleq \frac{\mathcal{R}_m(v)}{D_m}, \quad \forall m \in [M], \forall v \in [V] \tag{6}$$

Then, we formulate the optimization problem searching for any valid beam illumination pattern v. The process starts with proposals from the cell side, where satellite capacity constraints are not initially verified. Inspired by [13], we combine the weighted sum rate maximization with a sparsity penalty factor as the objective function for the sparsity-inducing regularization. The problem is defined as follows:

Problem 3:

$$\begin{aligned} \underset{\mathbf{a}_m}{\text{maximize}} \quad & \sum_{m\in[M]} \Big(R_m(\mathbf{a}_m) - \lambda_m \|\mathbf{a}_m\|_0 \Big) \\ \text{s.t.} \quad & \|\mathbf{a}_m\|_2^2 \le |\mathcal{F}_m|, \ \forall m \in [M] \qquad (7a) \\ & 0 \le a_{m,p} \le 1, \ p \in \mathcal{F}_m, \ \forall m \in [M] \qquad (7b) \end{aligned}$$

Note that $a_{m,p} \in \{0,1\}$ have been relaxed into continuous variables with box constraints, as shown in (7b). Now, we aim to select which cells are activated for each valid pattern and determine the number of active connections for each cell.

We address the first term—the weighted sum-rate formulation of our objective function by applying Quadratic Fractional Programming (QFP) [14]. We introduce two auxiliary variables γ_m and y_m to decouple the cell-specific variables due to the SINR expression. To deal with the sparsity penalty term, the discrete l_0-norm is relaxed into a surrogate. Because the subsequent deferred-acceptance step rounds variables back to $\{0,1\}$, we therefore adopt a reweighted-l_1-norm [15], a closer proxy to l_0-norm than the plain l_1-norm, thereby reducing the errors. By substituting the two terms, the objective function can be written as:

$$\begin{aligned} & \sum_{m\in[M]} \Big(\omega_m \log(1+\gamma_m) - \omega_m \gamma_m \\ & + 2y_m \sqrt{\omega_m(1+\gamma_m) \left(\sum_{p\in\mathcal{F}_m} a_{m,p}^2 |h_{m,p}|^2 \right)} - y_m^2 \sigma^2 \\ & - \sum_{j\in[M]} y_j^2 \mathbf{a}_m^T \mathrm{diag}\left\{ \mathbf{h}_{j,\mathcal{F}_m}^* \odot \mathbf{h}_{j,\mathcal{F}_m} \right\} \mathbf{a}_m \\ & - \lambda_m \|\alpha_m^T \mathbf{a}_m\| \Big) \end{aligned} \tag{8}$$

For each cell m, setting the gradient of the objective function to zero yields the closed-form solution for updating elements of $\mathbf{a}_m$:

$$a_{m,p} = \begin{cases} 0, & u_{m,p} \le \lambda_m, \\ \frac{(u_{m,p} - \lambda_m \alpha_{m,p})}{J_{m,p}}, & 0 \le \frac{(u_{m,p} - \lambda_m \alpha_{m,p})}{J_{m,p}} \le 1, \ u_{m,p} \ge \lambda_m, \\ 1, & \frac{(u_{m,p} - \lambda_m \alpha_{m,p})}{J_{m,p}} \ge 1, \ u_{m,p} \ge \lambda_m, \end{cases} \tag{9}$$

We define $\mathbf{u}_{m,\mathcal{F}_m} = 2y_m \sqrt{\omega_m(1+\gamma_m)} \mathbf{h}_{m,\mathcal{F}_m}$ and $\mathbf{J}_{m,\mathcal{F}_m} = \sum_{j\in[M]} y_j^2 \mathbf{h}_{j,\mathcal{F}_m}^* \circ \mathbf{h}_{j,\mathcal{F}_m}$, with $u_{m,p}$ and $J_{m,p}$ inferred from above [13]. The weighted vector elements are updated by:

$$\alpha_{m,p} = \frac{1}{a_{m,p}^2 + 1} \tag{10}$$

TABLE I
PARAMETER UPDATE PROCEDURE

Step	Operation
1	Update $\mathbf{u}_{m,\epsilon_m}$.
2	Update $\mathbf{J}_{m,\epsilon_m}$.
3	Update γ_m.
4	Update $\mathcal{R}_m$ using γ_m.
5	Update η and $\Delta\eta$ using η^{prev} and $\Delta\eta^{\text{prev}}$.
6	Reset $[\underline{\lambda_m}, \overline{\lambda_m}]$.

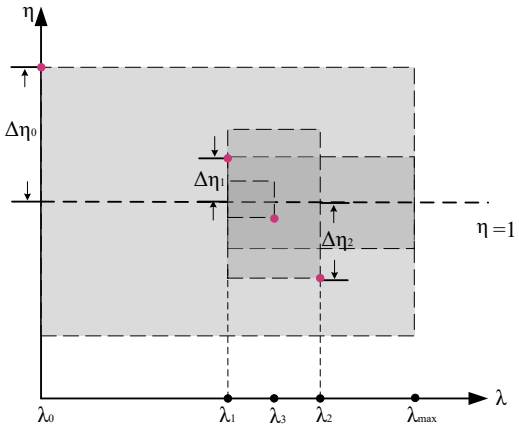


Fig. 2. Geometric Illustration of the Two-Dimensional Bisection Search.

Unlike [13], we design a 2D-bisection search method, shown as Algorithm 1, to control the sparsity of $\mathbf{a}_m$, and steer the achievable capacity $\mathcal{R}_m$ toward D_m. The search for λ_m can be interpreted geometrically in the (λ_m,η_m) plane, where the target condition is $\eta_m = 1$, as illustrated in Fig. 2. The update is encoded by four binary flags that indicate the two consecutive states with respect to $\eta_m = 1$, whether the new state moves closer to this partition line, and which interval boundary should be updated. The key invariant is that the shrinking rectangle always contains $\eta_m = 1$, while the interval of λ_m shrinks monotonically.

To generate sparse multi-connectivity beam patterns, we propose a Recursive Pattern Search algorithm shown in Algorithm 2 and Algorithm 3, with probing and pruning mechanisms. A Gauss-Seidel update incrementally probes cells via Algorithm 1, yielding sparse activation and avoiding cyclic updates. In each recursion, a candidate cell $m \in \mathcal{M}_{cd}$ is selected and computed via Algorithm 1. The current state S_{bkp} is saved, including γ and y, before adding m. If adding m causes any active cell $i \in \mathcal{M}_{ac}$ to violate $\mathcal{R}_i \le \eta_{\text{th}} D_i$, the state is restored and m is discarded; otherwise, m is added and the state is updated.

Forward pruning further trims the candidate set, based on cell m's beam overlapped count b_m, according to the following rule: If $b_m < \beta_1$, only the cell itself is removed from $\mathcal{M}_{cd}$; if

Algorithm 1 2D-Bisection Search for Demand Matching

Initialize $a_{m,p} \leftarrow 1$, $\alpha_{m,p} \leftarrow 1$, $\forall p \in \mathcal{F}_m$, set iteration index $i \leftarrow 0$, and maximum iteration number I_{iter}.
Call Table I.
repeat
  Set $\lambda_m \leftarrow (\overline{\lambda_m} + \underline{\lambda_m})/2$.
  Update $a_{m,p}$, $\forall p \in \mathcal{F}_m$, using (9).
  Update $\alpha_{m,p}$, $\forall p \in \mathcal{F}_m$, using (10).
  if the support set unchanged for $K_{\max}$ **then**
    $\mathbf{a}_m^{(i)} \leftarrow \mathbf{a}_m^{(i-K_{\max})}$.
    Call Table I.
  else
    Update γ_m.
    Update $\mathcal{R}_m$ using γ_m.
    Update η^{new} and $\Delta\eta^{\mathsf{new}}$.
    Reset $[\underline{\lambda_m}, \overline{\lambda_m}]$ using binary flags.
    Set $\eta^{\mathsf{prev}} \leftarrow \eta^{\mathsf{new}}$.
  end if
  Set $i \leftarrow i + 1$.
until $i \geq I_{iter}$.

$\beta_1 \leq b_m \leq \beta_2$, cell m and its first-tier neighbors $\mathcal{M}_1(m)$ are removed; if $b_m > \beta_2$, all cells up to second-tier neighbors of cell m are removed, based on hexagonal adjacency.

Recursion terminates when feasibility is violated, or the candidate set becomes empty, or reaches the recursion depth I_{L}. Valid patterns finally form the set $[V]$.

Algorithm 2 Recursive Pattern Search

Require: System model including cell set $[M]$, satellite set $[N]$, channel state for each cell $h_{m,\mathcal{F}_m}$, $\forall m \in [M]$, and traffic demand of each cell D_m, $\forall m \in [M]$.
Ensure: Pattern $[V]$.
Initialize active set $\mathcal{M}_{ac} \leftarrow \emptyset$, candidate set $\mathcal{M}_{cd} \leftarrow [M]$, solution set $[V] \leftarrow \emptyset$, and state S with zeros.
Set recursive level $l \leftarrow 1$.
RecursiveSearchProcedure$(\mathcal{M}_{ac}, \mathcal{M}_{cd}, S, I_L)$.

To reduce the problem complexity, we divide $[M]$ through grouping. In D2C scenarios, cells exhibit heterogeneous demands. The grouping strategy mixes high- and low-demand cells to balance resource usage and reduce mutual interference. The algorithm first sorts all cells by demand. At each iteration, cells are grouped from the front and back. The process repeats until each cell has been assigned to exactly one group (i.e., $[M] \rightarrow \{\mathcal{M}_q\}_{q=1}^{G}$). Each group acts as an input into Algorithm 2 instead of the original $[M]$.

B. Deferred Acceptance Matching Algorithm

After the cell-proposed scheme, high-demand cells draft more proposals to increase their chances of being served. Satellite then checks its capacity (2a). However, if satellites finalize connections prematurely, this can lead to first-mover advantages and reduced overall utility. To mitigate this, we employ a Deferred Acceptance Matching Algorithm, where satellites finalize decisions only after receiving all proposals.

Algorithm 3 RecursiveSearchProcedure

Require: Active set $\mathcal{M}_{ac}$, candidate set $\mathcal{M}_{cd}$, state S, maximum depth I_L
Ensure: Pattern $[V]$.
if $\mathcal{M}_{cd} = \emptyset$ **or** $l \geq I_L$ **then**
  Add pattern $(\mathcal{M}_{ac}, \mathbf{a}_m, m \in \mathcal{M}_{ac})$ to $[V]$.
  return
end if
for each candidate cell $m \in \mathcal{M}_{cd}$ **do**
  Save current state S_{bkp}.
  Compute cell m beam assignment using Algorithm 1.
  if feasibility is violated **then**
    Restore $S \leftarrow S_{\text{bkp}}$.
    continue
  end if
  Update active set: $\mathcal{M}'_{ac} \leftarrow \mathcal{M}_{ac} \cup \{m\}$.
  Update state $S' \leftarrow S$, $\forall j \in \mathcal{M}_{ac}$.
  Update $\mathcal{M}'_{cd}$.
  RecursiveSearchProcedure$(\mathcal{M}'_{ac}, \mathcal{M}'_{cd}, S', l+1)$.
  Restore $S \leftarrow S_{\text{bkp}}$.
end for

Each cell concurrently sends proposals according to $\mathbf{a}_m$. Then, each satellite n aggregates received proposals to form its global candidate proposal set:

$$\mathcal{Q}_\infty(n) = \bigcup_{m=1}^{M} \mathcal{Q}_m(n) = \bigcup_{m=1}^{M} \{(m, a_{m,n}) \mid a_{m,n} > 0\}. \quad (11)$$

where $a_{m,n}$ in $\mathcal{Q}_\infty(n)$ corresponds to the strength cell m's proposal to satellite n. Each satellite n selects the top Q_n strongest proposals from $\mathcal{Q}_\infty(n)$ to form its matching set $A_\infty(n)$. Formally, the satellite-side matching process is described as:

$$A_\infty(n) = \arg \max_{S \subseteq \mathcal{Q}_\infty(n), |S| \leq Q_n} \sum_{(m,a_{m,n}) \in S} a_{m,n}. \quad (12)$$

If fewer than Q_n proposals are received, all are accepted. Optimality follows from the fact that complete sets dominate any partial set [12].

After matching decisions are finalized, the binary connection state $x_{m,n}^v$ indicating whether satellite n serves cell m in pattern v is determined.

C. Complexity Analysis

Front–back cell grouping only requires sorting the M cells and partitioning them into G groups, which is $O(M \log M)$. The recursive pattern search with the bisection-based demand matching subroutine generates at most V valid patterns, with a per-iteration cost that is linear in the maximum number of visible satellites $F = \max_{m \in [M]} |\mathcal{F}_m|$. The subsequent deferred-acceptance matching then processes each pattern with a polynomial complexity in N, F, and V, by selecting the strongest proposals under each beam-capacity constraint.

Algorithm 4 Deferred Acceptance Matching Algorithm

Require: Valid pattern $[V]$.
Ensure: Connection state $x_{m,n}^{v}$, $v \in [V]$.

1: **Initialization:** Extract active cells and $\mathbf{a}_m^{(v)}$ from each valid pattern v.
2: **for** each cell m **in parallel do**
3: Send proposals concurrently to satellites.
4: **end for**
5: **for** each satellite n **in parallel do**
6: Aggregate received proposals into $\mathcal{Q}_\infty(n)$ by (11).
7: Form final matching set $A_\infty(n)$ by (12).
8: Determine the connection state.
9: **end for**

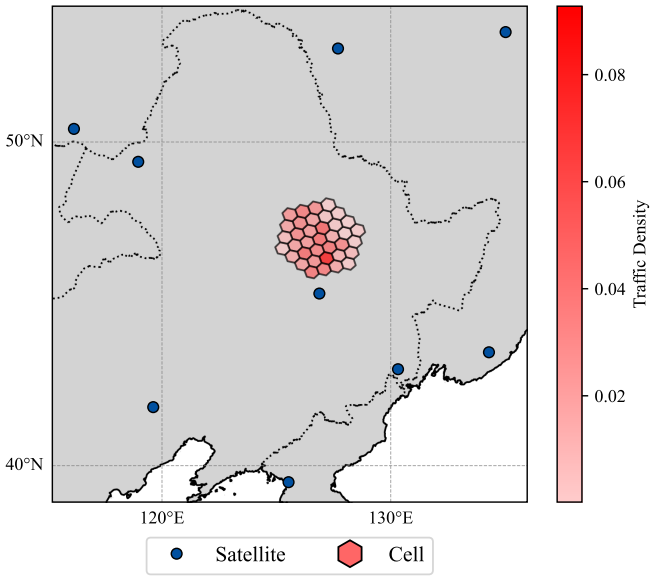


Fig. 3. Visualization of a Phase-1 constellation snapshot, with only the visible subset ($\epsilon \geq 30°$) shown, and the normalized traffic demand heat map derived from geographic population density.

Finally, the MILP scheduler operates on the reduced pattern set $[V]$ instead of the full combinatorial space; since $V \ll \prod_{n=1}^{N} \sum_{k=0}^{Q_n} \binom{|\tilde{\mathcal{F}}_n|}{k}$, $[V]$ can be viewed as a sparsely sampled subset that guides the solver toward more efficient search directions.

IV. Numerical Results

A. Simulation Setups

The satellite constellation is configured according to SpaceX's FCC filings for Starlink Direct-to-Cell constellation, currently the most ambitious D2C deployment plan. It includes 840 satellites in Phase-1, expanding to 2016 in Phase-2, arranged in two shells: One at 53°/530 km, the other at 43°/520 km. Each shell employs a 14-plane Walker-Delta constellation. Satellite snapshots are generated from ten snapshots at 6 s intervals.

We consider 37 hexagonal cells in Heilongjiang Province, China, each approximately 26 km in diameter (H3 resolution 4

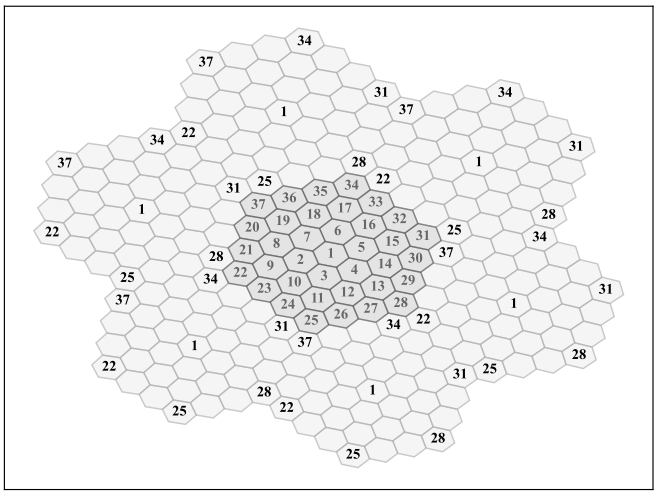


Fig. 4. The hexagonal cells after wrap-around.

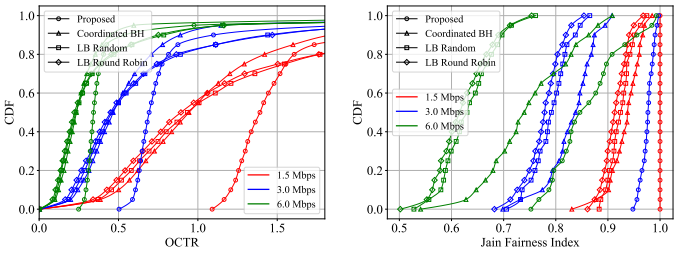
[16]). To eliminate boundary effects, wrap-around processing for hexagonal grids is employed [17]. The elevation threshold for satellite visibility is 30°. The average number of UEs per cell is set to 5, with traffic distributions derived from population density [18]. The generated user count per cell is clipped to [0,80] users, considering 30 MHz bandwidth, with B_{RB} = 180 kHz and N_{RB} = 160. Per-cell demand equals the user count times the traffic density. Channel parameters are generated using suburban/rural NTN settings, with the satellite-to-cell channel modeled as the average over users in the cell. Link budget parameters follow 3GPP NTN Set-1 for 600km altitude [19]. The scheduling period consists of T = 100 NR slots. The MILP solver [20] exploration count is limited to N_{exp} = 100,000.

B. Performance Analysis

We perform 80 Monte Carlo runs, each using a randomly selected satellite snapshot. The proposed multi-connectivity design uses $[\beta_1,\beta_2]$=[1,4], I_L=$\lceil |\mathcal{M}_q|/4 \rceil$, $\eta_{\text{th}} = 0.99$, and $Q_n = \max\{1, \lceil |\tilde{\mathcal{F}}_n|/2 \rceil\}$, compared with single-connectivity methods, including coordinated BH scheme [2], Load-Balancing Random Scheduling(LB Random) and Load-Balancing Round Robin(LB Round Robin). Both LB Random and LB Round Robin schemes first adopt the greedy load-balancing satellite-cell association from [2], avoiding illuminating beams toward cells without any traffic, and then, for each satellite, beams are scheduled randomly or periodically. For single-connectivity cases, each satellite illuminates $Q_n = \max\{1, \lceil M_n/4 \rceil\}$ beams for each pattern [2].

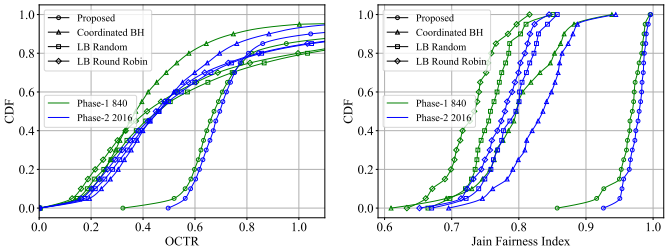
We assess system performance using the OCTR metric across cells in all setups. Additionally, we adopt the Jain fairness index over the OCTR metric with non-zero demand within each simulation setup, defined as:

$$I_{\mathcal{J}} = \frac{\left(\sum_{i \in \mathcal{M}_{nz}} \eta_i\right)^2}{|\mathcal{M}_{nz}| \sum_{i \in \mathcal{M}_{nz}} \eta_i^2}, \tag{13}$$



(a) OCTR comparison (b) $I_{\mathcal{J}}$ comparison

Fig. 5. Multi- vs. single-connectivity at varying traffic density.



(a) OCTR comparison (b) $I_{\mathcal{J}}$ comparison

Fig. 6. Multi- vs. single-connectivity under different constellation configurations.

where $\mathcal{M}_{nz}$ is the set of cells with non-zero demand. $I_{\mathcal{J}}$ closer to 1 indicate a more egalitarian schedule scheme. The analysis adopts the Phase-2 constellation, unless otherwise noted.

Fig. 5 evaluate the impact of increasing traffic density $\{1.5, 3.0, 6.0\}$ Mb/s/user, representing 3G-level service. The proposed multi-connectivity scheme consistently achieves better OCTR and $I_{\mathcal{J}}$. As traffic density increases, all methods degrade, and the performance gap narrows. Multi-connectivity provides higher throughput and fairness under moderate traffic. The gain stems from the spatial degrees of freedom by multi-satellite multi-connectivity, allowing the MILP solver to adapt slot-occupancy to better match heterogeneous demand; however, this advantage decreases substantially once demand exceeds the peak rate, even under multi-satellite concentrated beam illumination.

Fig. 6 evaluate the performance impact of enlarging the constellation from Phase-1 to Phase-2. For OCTR and $I_{\mathcal{J}}$, all the benchmarks see modest improvement with the denser constellation. Counterintuitively, the proposed multi-connectivity method exhibits negligible performance gains, primarily because a larger constellation provides more opportunities to connect with nearby satellites in a snapshot. For the proposed method, additional satellites enable a greater beam overlapped count. However, the rise in beam overlapped count also intensifies inter-beam interference, which in turn constrains the throughput that each beam illumination pattern can deliver.

V. Conclusion

This paper presented a beam scheduling method enabling multi-connectivity in multi-satellite NTN LEO D2C systems. A cell-proposed deferred acceptance matching scheme was developed to generate sparse patterns for input to an MILP solver. Simulation results confirm that the proposed approach improves fairness and provides better demand matching compared with the single-connectivity benchmarks. These findings show that multi-connectivity improves demand matching and fairness in the studied NTN D2C deployment setting.

References

[1] G. Taricco and A. Ginesi, "Precoding for flexible high throughput satellites: Hot-spot scenario," *IEEE Transactions on Broadcasting*, vol. 65, no. 1, pp. 65–72, 2018.

[2] Z. Lin, Z. Ni, L. Kuang, C. Jiang, and Z. Huang, "Multi-satellite beam hopping based on load balancing and interference avoidance for ngso satellite communication systems," *IEEE Transactions on Communications*, vol. 71, no. 1, pp. 282–295, 2022.

[3] M. Y. Abdelsadek, G. Karabulut-Kurt, H. Yanikomeroglu, P. Hu, G. Lamontagne, and K. Ahmed, "Broadband connectivity for handheld devices via leo satellites: Is distributed massive mimo the answer?" *IEEE Open Journal of the Communications Society*, vol. 4, pp. 713–726, 2023.

[4] X. Zhang, S. Sun, M. Tao, Q. Huang, and X. Tang, "Multi-satellite cooperative networks: Joint hybrid beamforming and user scheduling design," *IEEE Transactions on Wireless Communications*, vol. 23, no. 7, pp. 7938–7952, 2024.

[5] Z. Xu, G. Chen, R. Fernandez, Y. Gao, and R. Tafazolli, "Enhancement of direct leo satellite-to-smartphone communications by distributed beamforming," *IEEE Transactions on Vehicular Technology*, 2024.

[6] S. Yuan, Y. Sun, M. Peng, and R. Yuan, "Joint beam direction control and radio resource allocation in dynamic multi-beam leo satellite networks," *IEEE Transactions on Vehicular Technology*, vol. 73, no. 6, pp. 8222–8237, 2024.

[7] E. Bodine-Baron, C. Lee, A. Chong, B. Hassibi, and A. Wierman, "Peer effects and stability in matching markets," in *International Symposium on Algorithmic Game Theory*. Springer, 2011, pp. 117–129.

[8] *NR; Physical Channels and Modulation*, document 3GPP TS 38.211, V18.3.0, Release 18, Jul. 2024.

[9] T. R. Speidel and A. J. Gerber, "Method and apparatus for handling communications between spacecraft operating in an orbital environment and terrestrial telecommunications devices that use terrestrial base station communications," sep 2018, uS Patent 10,084,535.

[10] H. A. Ammar, R. Adve, S. Shahbazpanahi, G. Boudreau, and K. V. Srinivas, "Downlink resource allocation in multiuser cell-free mimo networks with user-centric clustering," *IEEE Transactions on Wireless Communications*, vol. 21, no. 3, pp. 1482–1497, 2021.

[11] A. Wang, L. Lei, E. Lagunas, A. I. Pérez-Neira, S. Chatzinotas, and B. Ottersten, "Noma-enabled multi-beam satellite systems: Joint optimization to overcome offered-requested data mismatches," *IEEE Transactions on Vehicular Technology*, vol. 70, no. 1, pp. 900–913, 2020.

[12] E. A. Jorswieck, "Stable matchings for resource allocation in wireless networks," in *2011 17th International Conference on Digital Signal Processing (DSP)*. IEEE, 2011, pp. 1–8.

[13] M. Hong, R. Sun, H. Baligh, and Z.-Q. Luo, "Joint base station clustering and beamformer design for partial coordinated transmission in heterogeneous networks," *IEEE Journal on Selected Areas in Communications*, vol. 31, no. 2, pp. 226–240, 2013.

[14] K. Shen and W. Yu, "Fractional programming for communication systems—part ii: Uplink scheduling via matching," *IEEE Transactions on Signal Processing*, vol. 66, no. 10, pp. 2631–2644, 2018.

[15] E. J. Candes, M. B. Wakin, and S. P. Boyd, "Enhancing sparsity by reweighted ℓ_1 minimization," *Journal of Fourier analysis and applications*, vol. 14, pp. 877–905, 2008.

[16] U. T. Inc., *Uber Engineering Blog*, Jun. 2018, [Online]. Available: https://www.uber.com/blog/h3/.

[17] A. Patel, *Hexagonal Grids*, 2013, [Online]. Available: https://www.redblobgames.com/grids/hexagons/#wraparound.

[18] K. Inc., *Geospatial Datasets Catalog*, [Online]. Available: https://www.kontur.io/datasets/#population.

[19] *Solutions for NR to Support Non-Terrestrial Networks (NTN)*, document 3GPP TR 38.821, V16.1.0, Release 16, May 2021.

[20] L. Gurobi Optimization, *Gurobi Optimizer Reference Manual*, 2024, [Online]. Available: https://www.gurobi.com.